A Journal of the Gesellschaft Deutscher Chemiker

Angewandte International Edition GDCh Chemie

www.angewandte.org

Accepted Article

Title: An Amphiphilic Cell-Penetrating Macrocycle for Efficient Cytosolic Delivery of Proteins, DNA and CRISPR Cas9

Authors: Somayah Qutub, Imtiyaz Bhat, Batoul Maatouk, Basem Moosa, Kashif Nawaz, Escarlet Diaz Galicia, Aliyah Fakim, Weibin Lin, Raik Grünberg, Stefan Arold, and Niveen M. Khashab

To be cited as: *Angew. Chem. Int. Ed.* **2024**, e202403647

Link to VoR: https://doi.org/10.1002/anie.202403647

WILEY VCH

10.1002/anie.202403647

WILEY VCH

RESEARCH ARTICLE

An Amphiphilic Cell-Penetrating Macrocycle for Efficient Cytosolic Delivery of Proteins, DNA, and CRISPR Cas9

Somayah S. Qutub[+],[a] Imtiyaz Ahmad Bhat[+],[a][b] Batoul I. Maatouk,[a] Basem Moosa,[a] Aliyah Fakim,[a] Kashif Nawaz,[c] Escarlet Diaz-Galicia,[d] Weibin Lin,[a] Raik Grünberg,[d] Stefan T. Arold,[d] Niveen M. Khashab,*[a]

[a] S. Qutub, Dr. I. Bhat, B. Maatouk, B Moosa, A. Fakim, Dr. W. Lin, Prof. N. Khashab
Smart Hybrid Materials (SHMs) Laboratory, Chemistry Program
King Abdullah University of Science and Technology (KAUST)
Thuwal. 23955-6900, Saudi Arabia
E-mail: niveen.khashab@kaust.edu.sa

[b] Dr. I. Bhat
Current Address: Department of Chemistry
Islamic University of Science and Technology
Awantipora, 192122, Jammu and Kashmir, India

[c] Dr. K. Nawaz
The Coral Symbiomics Lab, Red Sea Research center
King Abdullah University of Science and Technology (KAUST)
Thuwal 23955-6900, Kingdom of Saudi Arabia

[d] E. Diaz-Galicia, DR. R. Grünberg, Prof. S. Arold
Computational Bioscience Research Center (CBRC)
King Abdullah University of Science and Technology (KAUST)
Thuwal, 23955-6900, Saudi Arabia

Abstract: The discovery of safe platforms that can circumvent the endocytic pathway is of great significance for biological therapeutics that are usually degraded during endocytosis. Here we show that self-assembled and dynamic macrocycles can passively diffuse through the cell membrane and deliver a broad range of biologics including proteins, CRISPR Cas9 and ssDNA directly to the cytosol while retaining their bioactivity. Cell penetrating macrocycle (**CPM**) can be easily prepared from the room temperature condensation of diketopyrrolopyrrole lactams with diamines. We attribute the high cellular permeability of **CPM** to their amphiphilic nature and chameleonic properties. They adopt conformations that partially bury polar groups and expose hydrophobic side chains thus self-assembling into micellar-like structures. Their superior fluorescence renders **CPM** trackable inside cells where they follow the endomembrane system. **CPM** outperformed commercial reagents for biologics delivery and showed high RNA knockdown efficiency of CRISPR Cas9. We envisage that this class of macrocycles will be an ideal starting point to design and synthesize biomimetic macrocyclic tags that can readily facilitate the interaction and uptake of biomolecules and overcome endosomal digestion.

Introduction

Many potential therapeutic applications of biologicals such as proteins and nucleic acids are held back by their fragility, poor cell membrane permeability or endo/lysosomal entrapment, which affect intracellular functioning.[1] Hence substantial interest has been directed to develop both viral and non-viral artificial transporters to deliver hydrophilic and relatively bulky bio-active cargos.[2] In comparison to viral vectors, which pose safety concerns and design limitations, non-viral gene delivery platforms such as synthetic ionophores [3], macrocycles [4], nanoparticles [5], counterion activators [6], liposomes [7] and most recently coordination based frameworks [8] have attracted much attention. However, the delivery efficiencies of most of these non-viral vectors remained low mainly due to their endosomal entrapment that leads to the enzymatic and acid degradation of the cargo before reaching the target.[9]

10.1002/anie.202403647

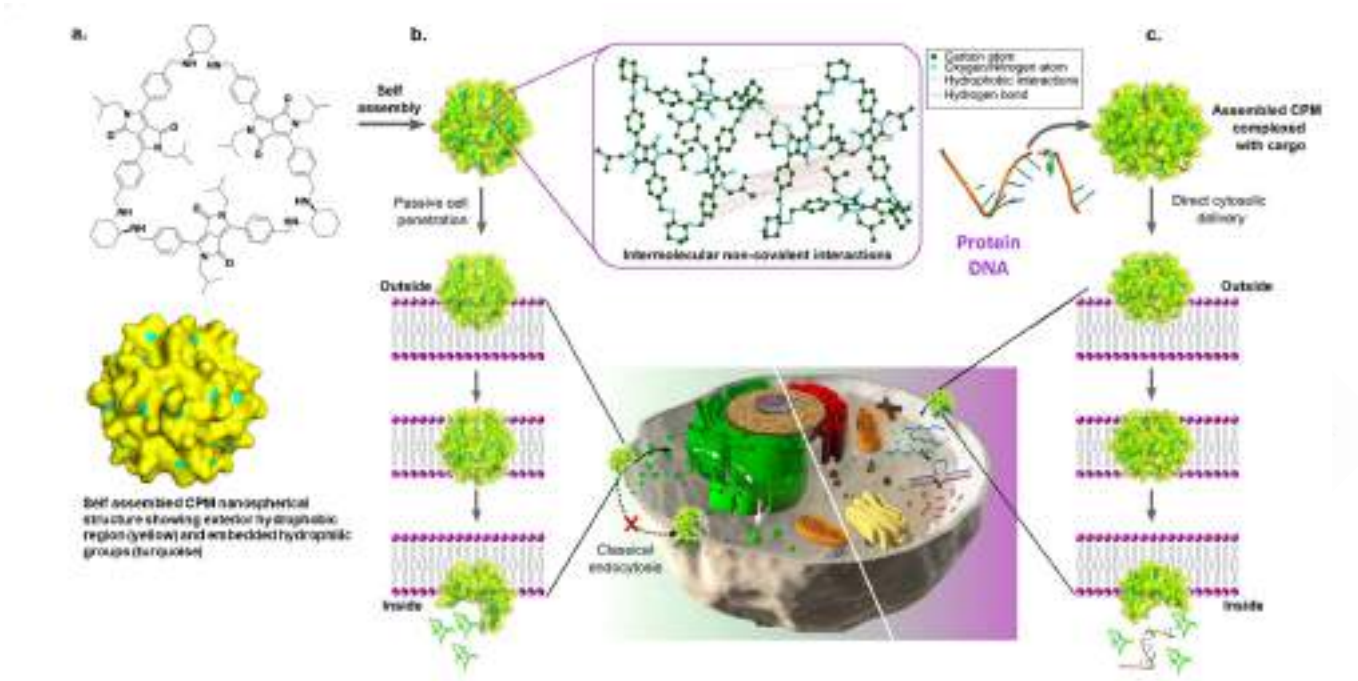

Figure 1. a. Chemical structure of **CPM. b.** Self-assembly of CPM molecules to form a nanospherical structure and its passage through the cell membrane. **c.** Complexation of DNA/RNA occupying the central space of self-assembled CPM spherical structure and their passage through the cell membrane.

Despite the ability of many of the engineered carriers to escape the endosomes, most of them are affected by the rupture and release of protease and hydrolase into the cytosol.[10] Since the discovery of the TAT peptide in 1988,[11] a broad variety of arginine-rich cell penetrating peptides (CPPs) and their mimics including polydisulfides have been adopted to evade endocytosis. Nonetheless, their mechanism of cytosolic delivery is still heavily debated as CPPs can enter mammalian cells via multiple mechanisms and direct permeation can happen only at low concentrations and promoted by the macrocyclic structure [12] In nature, we find that macrocyclic domains have always showed superior biomedical activity through favored proteins interactions. In fact, natural selection has clearly contributed to the evolution of macrocyclic secondary metabolites as they show improved target-ligand interactions.[13] The physical and chemical properties of macrocycles are unique and differ from their individual building blocks due to their supramolecular nature and 3D structure. Interestingly, one of the basic functional properties of macrocyclic domains, similar to protein domains, is their ability to assemble non-covalently with each other and to mediate the assembly of other macromolecules.[14] Cyclosporin A (CsA), is a natural cyclic peptide used medically as an immunosuppressant and is able to navigate through the ell membrane due to its dynamic self-assembled structure.[15] Moreover, Ascomycin, another macrocyclic peptide, which is also used as a strong immunosuppressant, showed an excellent interaction with cell membranes and proteins owing to the localization of the polar and non-polar functional groups along the circumference of the macrocycle.[16] Inspired by these natural macrocyclic systems, we designed and synthesized an amphiphilic flexible macrocycle that readily self assembles to passively diffuse through the cell membrane and can efficiently deliver proteins, and DNA directly to the cytosol. This cell penetrating macrocycle (CPM) can readily complex the biologics load through various non-covalent interactions and deliver these cargos to the cytosol efficiently (Figure 1). The CPM self-assembly is reminiscent of the self-assembly of nanoscale peptides [17] and non-covalent interactions of Amphotericin B monomers to form an octameric membrane pore.[18] Moreover, in contrast to the previously reported cyclic peptides that require tedious synthesis, [19] CPM can be prepared in high yield via a one-step condensation reaction starting from the biocompatible diketopyrrolopyrole (DPP) lactam.[20] DPP was originally chosen not only for its amphophilic nature but also due to its intense fluorescence which allows us to monitor CPM uptake and pathways inside cells. The design principle of CPM depends on incorporating polar and nonpolar groups that are capable of forming internal hydrogen bonds in a dynamic structure (Figure 1a-b). Previous investigation of macrocyclic peptides has demonstrated that passive membrane permeability is a feature of synthetic systems that can readily take up conformations with internally satisfied hydrogen bonding while permeability was hugely compromised when hydrogen-bonding groups were oriented towards the solvent.[21] The weak non-covalent interactions, such as hydrogen-bonding, electrostatic and

10.1002/anie.202403647

hydrophobic interactions, control the dynamic processes of membrane translocation of a carrier system. Therefore, supramolecular systems utilizing these non-covalent interactions are powerful tools to understand and develop conceptually smart non-viral delivery vectors.

Results and Discussion

Design and synthesis of CPMs

Over the years, DPP lactams with their outstanding photoluminescence (PL) properties have been used as fluorescent probes for various applications, such as detection of essential biological components, bio-imaging and even cancer therapy.[22] Their distinct structural features with the presence of two hydrophobic side chains and two lactam rings polar groups make them the ideal building blocks for an amphiphilic macrocycle.[14, 23] The chemical structure and synthetic route to the **CPM** are shown in supporting information Scheme S1. Starting with the DPP-aldehyde **(Ald)** (Figure S1-3), the target (3+3) **CPM** was synthesized through the Schiff base condensation reaction with (1R,2R)-(+)-1,2-Diaminocyclohexane L-tartrate followed by reduction with $NaBH_4$ (Scheme S1). The formation of **CPM** was confirmed by ^{1}H NMR, ^{13}C NMR and ESI-MS spectrometry (Figure S1-10). In the ^{1}H NMR, **CPM** displays two doublets in the aromatic region (7.79 and 7.52 ppm) due to its highly symmetrical cyclic structure (Figure S7). In the ^{13}C NMR spectrum, **CPM** gives 15 peaks in the aromatic region that can be assigned to the DPP core and cyclohexane diamine (Figure S8). All these results confirm the formation and the proper characterization of **CPM**. To gain more insight on the structural features of **CPM**, a diffusion ordered 2D NMR spectroscopy (DOSY) was performed, which showed a single diffusion coefficient (*D*) value of 3.4×10^{-10} m^2/s. This suggests that a single component is formed rather than a mixture of products (Figure S10).

Structurally, **CPM** consists of a heterocyclic dilactam macrocyclic scaffold with alternate hydrophilic region containing multiple C=O, NH, N-methylated groups and a hydrophobic region containing benzene, cyclohexane and long isopropyl side chains. Interestingly, this amphiphilic nature along with its flexible amine bonds, allows it to self-assemble into micellar-like secondary structures utilizing non-covalent intermolecular interactions in aqueous media and to readily interact with the biologics load (Figure 1b). To investigate the structural morphology of the self-assembled **CPM**, high-resolution transmission electron microscopy (HR -TEM), and atomic force microscopy (AFM), measurements were done, which confirmed the formation of micellar-like nanospherical structures (Figure 2a,b). To further analyze the surface properties of the **CPM** assembly, the zeta potential was measured to be +20 mV suggesting its cationic nature compared to the starting **(Ald)** (Figure 2d). As to the spectroscopic characterization, the fluorescence spectrum of Ald exhibits a maximum fluorescence band at 590 nm with a shoulder at approximately 625 nm upon excitation at a wavelength of 450 nm (Figure S11a). The introduction of the amine bond upon the formation of **CPM** shifts the emission wavelength to near 540 nm (Figure S11b). This blue shift observed in **CPM** is due to the loss of C=O π bond, thus, making **CPM** less conjugated compared to Ald. The physical properties of **CPM** were explored at different pH values and dilution degrees (Figure S11c). The fluorescence spectra did not show much change with respect to the change in the pH. However, upon dilution, the fluorescence emission peak changes from 580 to 540 nm (Figure 2 e,f). At a concentration of 40 μM, the **CPM** exhibited a fluorescence peak at 540 with a shoulder peak at 580 nm. Upon increasing the concentration to 90 μM, the **CPM** displayed aggregation caused quenching (ACQ) with a decreased single broad emission peak observed at 580 nm. The significance of this finding is that this fluorescence change can help monitor the uptake of the system by the cells, where a fluorescence shift towards 540 nm will be expected with more **CPM** diffusing through. Remarkably, **CPM** have a high quantum yield of 51% measured in reference to the standard Rhodamine 6G dye with significant two photon absorption cross-section of 24 (Figure S11d-e). The fluorescence decay was found to be strictly mono exponential and falling in the 5–6 ns range (Figure S12).

Cellular permeability

Before testing the permeability of **CPM**, we tested the biocompatibility of our synthetic platform. **CPM** showed a high biocompatibility of ≥ 200 μg ml^{-1} in HDFn and HeLa cells, which is considerably higher than the precursor **Ald** (Figure S13a-b) similar trends were observed with other cell lines as well (Table S1). We then Investigated the ability of the molecules to passively diffuse into live cells by testing their migration through a phospholipid-impregnated membrane from a donor compartment to an acceptor compartment in a parallel artificial membrane permeability (PAMPA) assay. As expected, **CPM** effectively passed through the membrane compared to **Ald** and the rigid Schiff-based imine macrocycle **(RM)** (Figure 3a, Figure S4-6). Prompted by the success in PAMPA, we tested the cellular uptake by incubating **CPM** using different concentrations as shown in Figure S14. **CPM** can be detected even at low concentration of 0.5μg ml^{-1}, however, 10 μg ml^{-1} was used in all

10.1002/anie.202403647

RESEARCH ARTICLE

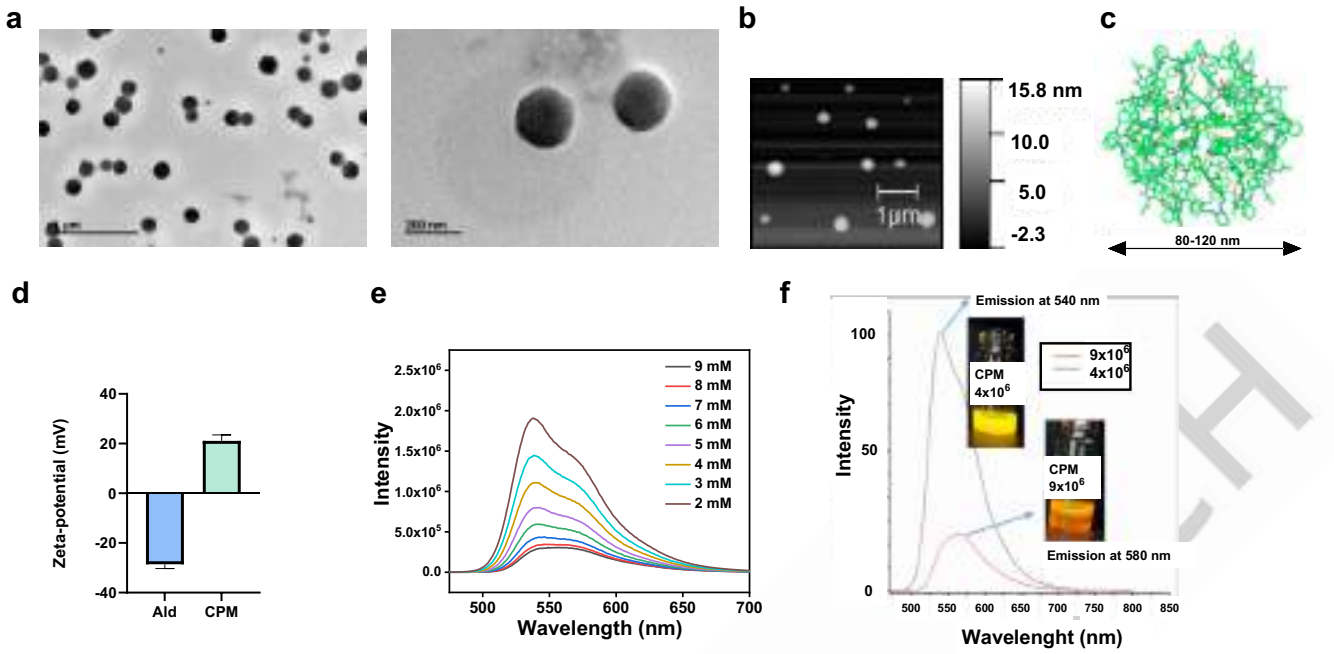

Figure 2. Self-assembly of **CPM**. **a.** TEM images**. b.** AFM images. **c.** Self-assembled **CPM** nanospherical structure obtained through *insilico* method. **d.** zeta-potential measurements of **Ald** and **CPM.** Error bars are based on SEM (n = 3). **e-f.** The change in fluorescence spectra of the **CPM** in THF upon dilution.

Subsequent experiments as it showed very bright green fluorescent within HeLa and nHDF cells. Moreover, a strong green fluorescence signal (Ex. 495 nm) inside the cells and an intense red fluorescence signal (Ex. 544 nm) from the aggregates outside can be clearly detected (Figure 3b). This indicates that the material possesses a blue-shifted excitation and emission spectra upon dispersion in cells, which supports our original findings when conducting the dilution experiments (Figure 2e-f).

More significantly, this observation greatly simplified the detection of the cellular uptake without the need to use Z-stack. As a control, 10 μg ml^{-1} of **Ald** were tested together with RM with HeLa and HDFn for which no fluorescence signals were detected inside the cells (Figure 3d & S15). This further proves that the dynamic and flexible structure of CPM plays a big role in its cellular permeability. The cellular uptake was quantified by the corrected total cells fluorescence intensity (CTCF) and by a spectrophotometer to measure the fluorescence in the cell lysate after 1h incubation with the molecules. These experiments confirmed the PAMPA results as **CPM** showed a stronger fluorescence signal in cells and cell lysate compared to **Ald** and **RM** (Figure 3a, c). To gain more insight into the uptake of **CPM** with HeLa cells, real time live imaging was implemented using CLSM. Within minutes, **CPM** exhibited a continuous increase in the intracellular green fluorescence signal with negligible background signal outside the cells (Video S1). Moreover, **CPM** had a distinct dynamic distribution patterns in the cytoplasm and perinuclear area; it showed a tendency to follow the endomembrane system that consists of endoplasmic reticulum (ER), Golgi apparatus, and lipid vesicles [24] (Figure 3e, Video S2). The fast uptake supports that **CPM** can enter the cell through passive diffusion, an energy-independent pathway.[10] To further examine the cellular uptake mechanism, the lipid-raft endocytosis pathway was inhibited using Methyl-β-cyclodextrin (MβCD).[25] MβCD did not affect the uptake of **CPM** in HeLa and HDFn cells after 30 minutes of incubation which supports our hypothesis towards the passive uptake (Figure S16a-b). Furthermore, we investigated the uptake of **CPM** with HeLa cells at low temperature (4°C) as it is known that all active cellular uptake is interrupted and only passive diffusion can occur below (10°C).[25] After 1hr of incubation, both cells incubated at 37 and 4°C showed a bright green fluorescence in the cytoplasm which further proved the passive diffusion and uptake of **CPM**. In addition, the green fluorescence was detected in the cytoplasm and Golgi apparatus at 37°C, whereas it was evenly distributed in the cytoplasm at 4°C confirming the dynamic properties of **CPM** as cellular activity is hindered at 4°C (Figure S17, S18). We took a step back to explore the mechanism of cellular uptake based on the structure of the **CPM** and its interaction with the plasma membrane. As postulated in the original design, the amphiphilic nature together with the ability to form internal hydrogen- bonding

10.1002/anie.202403647

RESEARCH ARTICLE

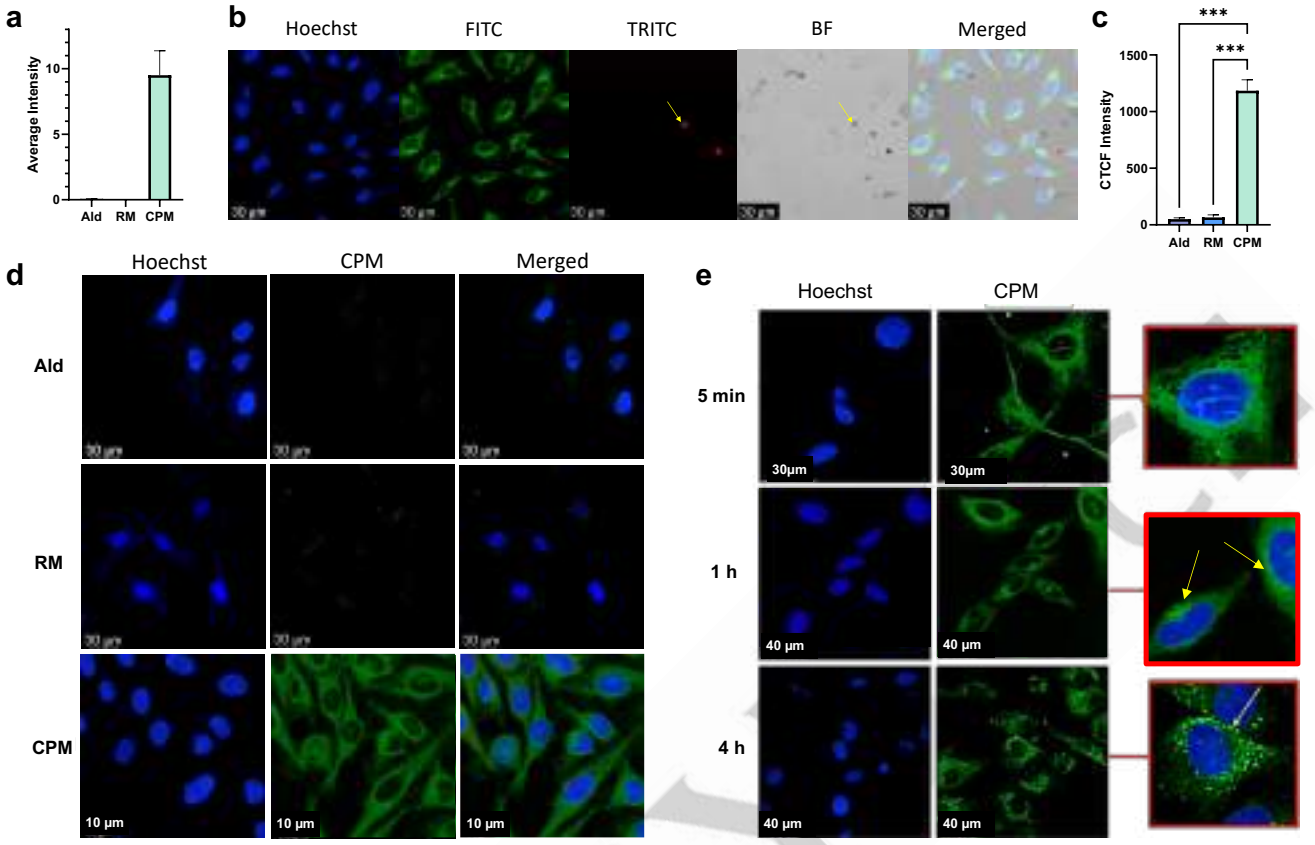

Figure 3. Permeability and cellular uptake. **a.** Fluorescence of the compounds were measured using fluorescence spectrophotometer in the acceptor well of the PAMPA assay after 24 hr. **b.** CLSM images of the uptake of 10 µg ml^{-1} of CPM with HeLa cells for 1 hr. FITC: Ex. 495 nm, Em. 520 nm and TRITC: Ex. 544, Em. 570 nm. The yellow arrow points to **CPM** aggregates outside the cells. **c.** Corrected Total Cells Fluorescence Intensity (CTCF) of the uptake of 10 µg ml^{-1} of **Ald**, **RM** and **CPM** with HeLa cells for 1 hr. **d.** CLSM images of the uptake of 10 µg ml^{-1} of **Ald**, **RM** and **CPM** with HeLa after 30 minutes. **e.** CLSM images of the uptake of 10 µg ml^{-1} of **CPM** with HeLa overtime. Error bars are based on SD (n = 4). Statistical significance was calculated by one-way ANOVA : *p < 0.05, **p < 0.01, ***p < 0.001, ****p < 0.0001.

assembly where the non-polar groups are positioned towards the outside while the polar groups are hydrogen-bonding towards the inside of the assembly (Figure 1a-b). Besides, it is crucial for large molecules with passive membrane permeability to have a flexible structure and ability to form internal hydrogen bonds. Therefore, the flexible structure of **CPM** in the presence of six N-H hydrogen bonding sites facilitated its diffusion through the plasma membrane mimicking the cyclic peptide cyclosporin A (CSA)[21b] . Thus, based on these results we concluded that the self-assembled **CPM** nanosphere translocate through the cell membrane initiated by first making the contact with the polar heads of the membrane through its surface polar N-H groups and then translocate through the lipid bilayer with the help of exterior hydrophobic groups (cyclohexyl and isopropyl groups).

Chaperoning proteins and DNA

Delivering biomolecules such as proteins and nucleic acids passively to the cytoplasm through endocytosis independent pathway (passive diffusion) possesses a great challenge mostly due to the cargos hydrophilic nature and large molecular weight which hinders their passive uptake.[26] After proving the passive diffusion of **CPM** across the cell membrane, we further checked the ability of **CPM** to chaperone biomacromolecules directly to the cytosol.[27] Thanks to its amphiphilic and flexible nature, **CPM** formed complexes with various proteins. We speculated that these complex assembled structures may be able to passively translocate protein cargos inside the cell. To test the delivery capability of CPM, we chose protein cargoes of different sizes and charges: mScarlet (26 kDa), bovine albumin serum (BSA) (66.5 kDa, negatively charged), lysozyme (14.3 kDa, positively charged), and a large protein-RNA complex (SauCas9-gRNA, 196 kDa). The negatively charged fluorescent protein, mScarlet,

10.1002/anie.202403647

RESEARCH ARTICLE

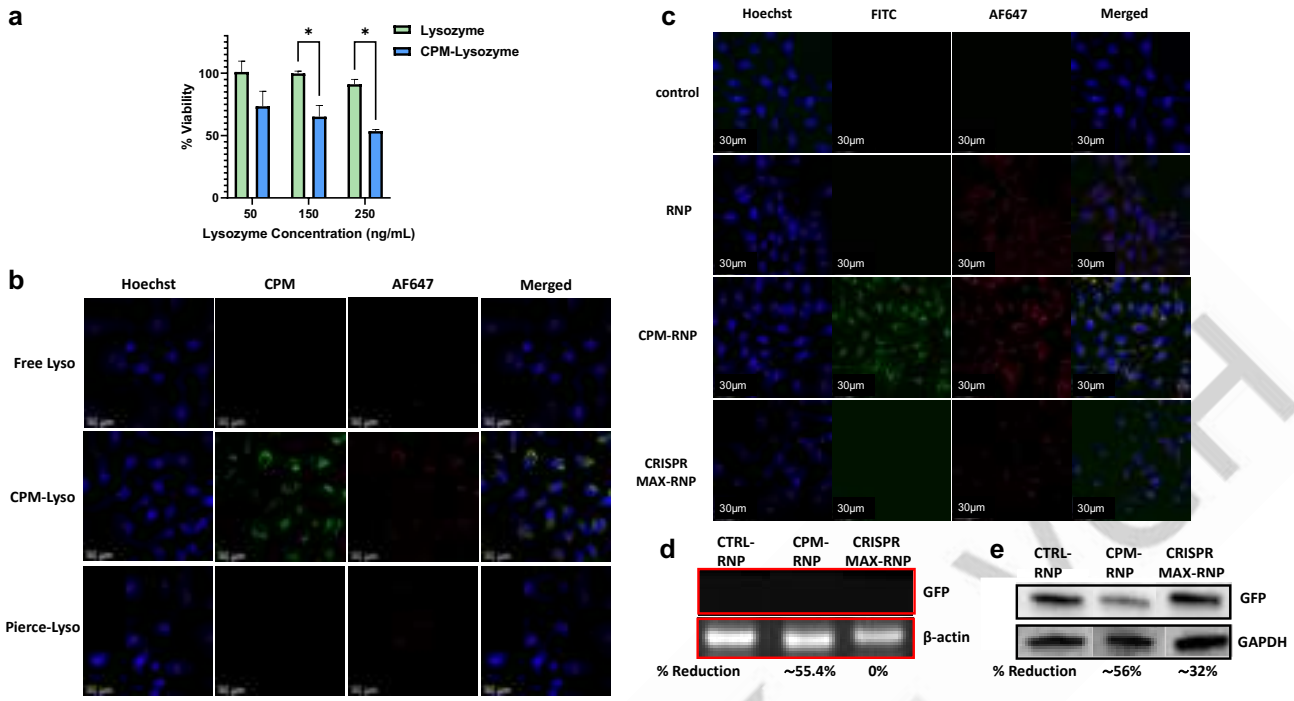

Figure 4. a. Cytotoxic effect on HeLa cells of lysozyme and CPM complex**. b**. CLSM images of HeLa cells treated with lysozyme, CPM-Lyso, and pierce-Lyso complex after 4hr. **c.** CLSM images of HeLa cells treated with RNP, and CRISPRMAX RNP. **d.** SDS agarose of the PCR products of GFP gene amplification after treatment of MCF-7-GFP cells with RNP, CPM- RNP, and CRIPRMAX RNP, β-actin was used as control (the bands were spliced from the full size gel Figure S21a). **e.** Western blot of GFP in GFP-labelled MCF-7 cells treated with RNP, CPM- RNP, and CRISPRMAX RNP to inhibit the expression of GFP protein, GAPDH was used as loading control (the bands were spliced from the full size blot Figure S21b). Error bars are based on SD (n = 4). Statistical significance was calculated by two-way ANOVA : * p < 0.05, **p < 0.01, ***p < 0.001, ****p < 0.000

[28] was complexed with **CPM** or a commercial protein transfection reagent (pierce) and incubated with HeLa cells for 4h. CPM-mScarlet showed a strong red fluorescent signal inside the cells whereas only a very faint signal was observed with the Pierce-transfected mScarlet. This suggested that **CPM** can deliver, and release negatively charged protein more efficiently than the commercial kit (Figure S19 a). We next investigated the uptake of a larger protein, BSA, labeled with Alexa Fluor 647 in complex with CPM. After 4 h incubation with HeLa cells, a strong red fluorescent signal was detected inside the cells whereas a only avery faint signal was observed with the free protein, confirming that **CPM** can deliver and release BSA inside HeLa cells (Figure S19b). We then investigated whether **CPM** delivery and release could maintain protein bioactivity, which would be crucial for protein-based therapeutic applications. Lysozyme has been reported to have an anti-proliferative effect on human cancer cells.[29] As shown in Figure 4a, the viability of cancer cells treated with CPM-lysozyme indeed decreased in comparison to lysozyme alone which indicates the efficient delivery and function of this protein within the cytosol. For comparison, the cellular uptake of Alexa Fluor647-labelled lysozyme was investigated using the Pierce reagent. As shown in Figure 4b, only CPM-Lysozyme showed a red fluorescent color inside of cells, indicating successful delivery. In summary, **CPM** can thus effectively complex with small and large proteins regardless of their charges, unlike the positively charged Pierce reagent which can complex and deliver only negatively charged proteins. Our next objective was to deliver and protect more delicate and complex cargo, such as the CRISPR Staphylococcus aureus Cas9 (SauCas9) ribonucleoprotein (RNP) [30] in complex with its guide RNA. Unlike regular Cas9 proteins, SauCas9 can be directed to cleave either specific DNA or RNA targets. For easier detection, we expressed SauCas9 as a fusion protein with the spyCatcher domain [31] which allowed us to autocatalytically assemble it with a separately purified mScarlet-I fluorescent protein featuring a matching spyTag. The overall molecular weight of this covalent SauCas9-spyCatcher-mScarlet fusion construct in (noncovalent) complex with a guide RNA comprised 196 kDa (170 kDa + guide RNA). **CPM** formed a nanospherical complex immediately upon the addition of mScarlet-labelled RNP which was confirmed by zeta-

10.1002/anie.202403647

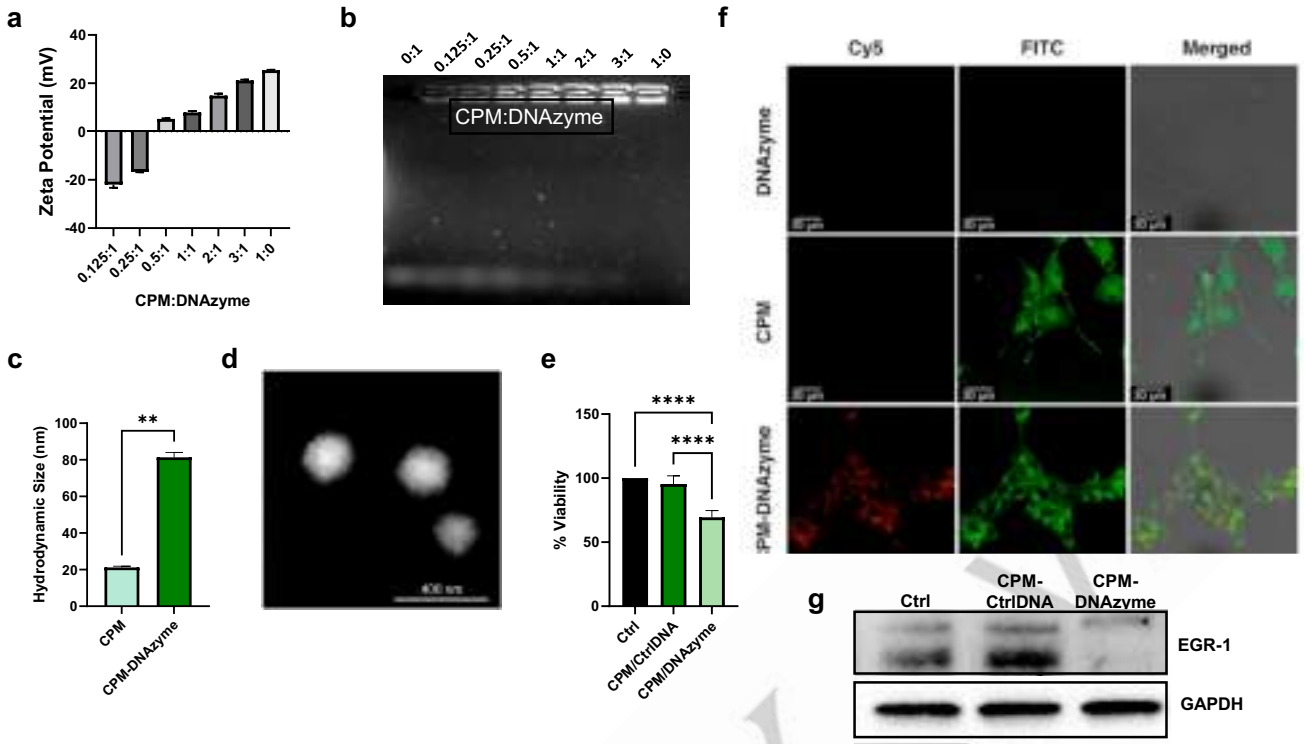

Figure 5. a. Zeta-potential measurements of CPM-DNAzyme complex while increasing the ratio of CPM to DNAzyme. **b.** Gel-Retardation assay for CPM with DNAzyme as it complexes in HEPES buffer. **c.** Hydrodynamic size of CPM and CPM-DNAzyme. **d**. AFM image of CPM-DNAzyme complex **e.** Cytotoxicity of Ctrl DNA, DNAzyme, CPM, and CPM-DNAzyme complex against MCF-7 cells. **f.** CLSM images of MCF-7 cells treated with labelled DNAzyme, CPM, and CPM-DNAzyme complex after 4hr. **g.** Western blot of EGR-1 protein in MCF-7 cells treated with Ctrl DNA, DNAzyme, CPM-Ctrl DNA,and CPM-DNAzyme to inhibit the expression of EGR-1, GAPDH was used as loading control (the bands were spliced from the uncropped image Figure S22). Error bars are based on SEM (n = 3). Statistical significance was calculated by one-way ANOVA and multiple comparisons test: (*, $p < 0.05$, **, $p < 0.01$, ***, $p < 0.001$, ****, $p < 0.0001$)

potential, hydrodynamic size, and AFM images (Figure S20 a-c). The zeta-potential decreased and the size of the molecule increased from 20 to 200 nm upon complexation of **CPM** with the RNP. We pre-loaded the SauCas9 with a guide RNA that targeted the mRNA of a green fluorescent protein (GFP) overexpression construct. The successful transport and intracellular release of the functional RNP complex would lead to a (non-permanent) knockdown of GFP expression without interfering with the cell's genome. We incubated HeLa and GFP-positive MCF-7 cells with RNP alone, the commercial transfection reagent CRISPRMAX, and with the CPM-RNP and followed the RNP distribution throughout HeLa cell as well as the expression of GFP in GFP-positive MCF-7 cells. As shown in Figure 4c, CPM-RNP gave the highest red fluorescent signal in the cytoplasm compared to free RNP and CRISPRMAX-RNP when incubated with HeLa cells.[32] More importantly, the level of mRNA decreased by about 55% with CPM-RNP whereas no significant difference was detected between CRISPRMAX-RNP and negative control after 48 h (Figure 4d). Indeed, CPM-RNP reduced the GFP protein expression by 56% outperforming CRISPRMAX which caused a 32% reduction (Figure 4e).Based on these experimental observations, we concluded that **CPM** efficiently delivered fully functional proteins into the cytosol regardless of their size, charge or complexity.

Inspired by the delivery of a protein – RNA complex, we proceeded to evaluate the delivery and function of a pure nucleic acid DNAzyme using the CPM. DNAzyme is a single stranded DNA (ssDNA) that binds to its target mRNA through Watson–Crick base pairing and cleaves the targeted mRNAs to inhibit their translation to protein. We targeted the early growth response (EGR-1) protein which is a growth factor that stimulates cell proliferation and chemotaxis [17]. First, we evaluated the interaction and complex formation between our system and ssDNA. The complexation of **CPM** with DNAzyme was investigated using gel-Retardation Assay. As shown in figure 5a, DNAzyme's zeta potential increased proportionally to the addition of **CPM** until it reached an equilibrium around 0.5:1 mass ratio of **CPM** to DNAzyme. Moreover, gel-Retardation Assay was used to further confirm the complexation between CPM-1 and DNA; the complexed structure would be retreated and no migration of DNA will be detected on the gel. As presented in Figure 5b, the DNA

10.1002/anie.202403647

within the complex did not migrate and was not detected on the gel. In order to investigate the structure of the assembled complex, AFM analysis was done and showed the formation of spherical nanostructures of size 80-120 nm which was consistent with the DLS measurement (Figure 5c-d)

The cellular uptake of the CPM-DNAzyme complex was investigated using CLSM and CY5 labelled DNAzyme. Fluorescent signal was detected after 4hr of incubation inside MCF-7 cells, whereas no signal was detected with free DNAzyme (Figure 5f). In order to prove the underlying gene silencing mechanism on the expression of EGR-1 protein, both active and inactive DNAzyme sequences were used. As presented in figure 5e-g, the CPM-DNAzyme caused a significant reduction of EGR-1 protein level and showed antiproliferative effect in MCF-7 cells with no reduction of EGR-1 protein level observed for cells treated with control DNA, CPM, and DNAzyme. These results suggest that the reduction in EGR-1 expression is caused by mRNA degradation upon the effective delivery of DNAzyme using the **CPM** as gene delivery vehicle.

Conclusion

A [3+3] fluorescent cell penetrating macrocycle **CPM** was obtained through Schiff base reaction using the DPP core unit. The *in vitro* studies using this macrocycle clearly demonstrate a remarkable cell penetration ability into both normal and cancer cells. The **CPM** macrocycle was effective for imaging and delivery at the nanomolar scale (300 nM) without any notable toxicity or interference with the cellular processes. Moreover, the self-assembled nanostructures based on the intermolecular hydrogen bonding were able to bind and deliver the RNP and DNAzyme cargos directly to the cytosol outperforming commercially available carriers. The macrocycle **CPM** exhibits outstanding dynamic fluorescence properties and passive cellular permeability mechanism rendering it a great candidate for imaging and drug delivery applications. Moreover, CPMs can efficiently deliver fully functional proteins and genetic materials into the cytosol regardless of their size, charge or complexity. We expect that such a class of self-assembled dynamic macrocycles will further our understanding of the factors that affect the cellular permeability of charged and large biological molecules.

Supporting Information

SI.pdf
Video1
Video2
The authors have cited additional references within the Supporting Information [35].

Acknowledgements

S.Q, and I.A.B contributed equally to this work

This work was supported by King Abdullah University of Science and Technology (KAUST).

Keywords: Biomimetic • Fluorescence • Passive delivery • Proteins • Self-assembly

10.1002/anie.202403647

References

[1] a) L. R. Baden, H. M. El Sahly, B. Essink, K. Kotloff, S. Frey, R. Novak, D. Diemert, S. A. Spector, N. Rouphael, C. B. Creech, J. McGettigan, S. Khetan, N. Segall, J. Solis, A. Brosz, C. Fierro, H. Schwartz, K. Neuzil, L. Corey, P. Gilbert, H. Janes, D. Follmann, M. Marovich, J. Mascola, L. Polakowski, J. Ledgerwood, B. S. Graham, H. Bennett, R. Pajon, C. Knightly, B. Leav, W. Deng, H. Zhou, S. Han, M. Ivarsson, J. Miller, T. Zaks, *New England Journal of Medicine* **2020**, *384*, 403-416; b) S. F. Dowdy, *Nature Biotechnology* **2017**, *35*, 222-229; c) R. Kanasty, J. R. Dorkin, A. Vegas, D. Anderson, *Nature Materials* **2013**, *12*, 967-977; d) S. Liu, Q. Cheng, T. Wei, X. Yu, L. T. Johnson, L. Farbiak, D. J. Siegwart, *Nature materials* **2021**, *20*, 701-710; e) A. L. Nelson, E. Dhimolea, J. M. Reichert, *Nat Rev Drug Discov* **2010**, *9*, 767-774; f) K. A. Whitehead, R. Langer, D. G. Anderson, *Nature reviews Drug discovery* **2009**, *8*, 129-138.

[2] a) M. Akishiba, T. Takeuchi, Y. Kawaguchi, K. Sakamoto, H.-H. Yu, I. Nakase, T. Takatani-Nakase, F. Madani, A. Gräslund, S. Futaki, *Nature chemistry* **2017**, *9*, 751-761; b) A. Barba-Bon, G. Salluce, I. Lostalé-Seijo, K. Assaf, A. Hennig, J. Montenegro, W. M. Nau, *Nature* **2022**, *603*, 637-642; c) R. G. Crystal, *Science* **1995**, *270*, 404-410; d) I. Lostalé-Seijo, J. Montenegro, *Nature Reviews Chemistry* **2018**, *2*, 258-277; e) G. Zuber, E. Dauty, M. Nothisen, P. Belguise, J. P. Behr, *Adv Drug Deliv Rev* **2001**, *52*, 245-253; f) J. Liu, T. Luo, Y. Xue, L. Mao, P. J. Stang, M. Wang, *Angewandte Chemie International Edition* **2021**, *60*, 5429-5435.

[3] a) P. A. Gale, J. T. Davis, R. Quesada, *Chemical Society Reviews* **2017**, *46*, 2497-2519; b) I. W. Park, J. Yoo, B. Kim, S. Adhikari, S. K. Kim, Y. Yeon, C. J. Haynes, J. L. Sutton, C. C. Tong, V. M. Lynch, J. L. Sessler, P. A. Gale, C. H. Lee, *Chemistry* **2012**, *18*, 2514-2523.

[4] a) C. O. Mellet, J. M. G. Fernández, J. M. Benito, *Chemical Society Reviews* **2011**, *40*, 1586-1608; b) F. Sansone, M. Dudič, G. Donofrio, C. Rivetti, L. Baldini, A. Casnati, S. Cellai, R. Ungaro, *Journal of the American Chemical Society* **2006**, *128*, 14528-14536.

[5] a) S. Behzadi, V. Serpooshan, W. Tao, M. A. Hamaly, M. Y. Alkawareek, E. C. Dreaden, D. Brown, A. M. Alkilany, O. C. Farokhzad, M. Mahmoudi, *Chem Soc Rev* **2017**, *46*, 4218-4244; b) R. Mout, M. Ray, G. Yesilbag Tonga, Y.-W. Lee, T. Tay, K. Sasaki, V. M. Rotello, *ACS Nano* **2017**, *11*, 2452-2458; c) F. Scaletti, J. Hardie, Y.-W. Lee, D. C. Luther, M. Ray, V. M. Rotello, *Chemical Society Reviews* **2018**, *47*, 3421-3432.

[6] a) M. Nishihara, F. Perret, T. Takeuchi, S. Futaki, A. N. Lazar, A. W. Coleman, N. Sakai, S. Matile, *Organic & Biomolecular Chemistry* **2005**, *3*, 1659-1669; b) N. Sakai, S. Matile, *Journal of the American Chemical Society* **2003**, *125*, 14348-14356.

[7] J. Gilleron, W. Querbes, A. Zeigerer, A. Borodovsky, G. Marsico, U. Schubert, K. Manygoats, S. Seifert, C. Andree, M. Stöter, H. Epstein-Barash, L. Zhang, V. Koteliansky, K. Fitzgerald, E. Fava, M. Bickle, Y. Kalaidzidis, A. Akinc, M. Maier, M. Zerial, *Nature Biotechnology* **2013**, *31*, 638-646.

[8] a) L. O. Alimi, M. Z. Alyami, S. Chand, W. Baslyman, N. M. Khashab, *Chemical Science* **2021**, *12*, 2329-2344; b) X. Wu, H. Yue, Y. Zhang, X. Gao, X. Li, L. Wang, Y. Cao, M. Hou, H. An, L. Zhang, S. Li, J. Ma, H. Lin, Y. Fu, H. Gu, W. Lou, W. Wei, R. N. Zare, J. Ge, *Nature Communications* **2019**, *10*, 5165; c) W. S. Baslyman, O. Alahmed, S. Chand, S. Qutub, N. M. Khashab, *Angew Chem Int Ed Engl* **2023**, *62*, e202302840.

[9] A. Fu, R. Tang, J. Hardie, M. E. Farkas, V. M. Rotello, *Bioconjug Chem* **2014**, *25*, 1602-1608.

[10] S. Du, S. S. Liew, L. Li, S. Q. Yao, *J Am Chem Soc* **2018**, *140*, 15986-15996.

[11] a) S. Lee, N. G. Housden, S. A. Ionescu, M. H. Zimmer, R. Kaminska, C. Kleanthous, H. Bayley, *J Am Chem Soc* **2020**, *142*, 12157-12166; b) F. Milletti, *Drug Discov Today* **2012**, *17*, 850-860.

[12] S. Futaki, I. Nakase, *Accounts of Chemical Research* **2017**, *50*, 2449-2456.

[13] H. Zhang, S. Chen, *RSC Chemical Biology* **2021**,3, 18-31.

[14] R. Breinbauer, I. R. Vetter, H. Waldmann, *Angewandte Chemie International Edition* **2002**, *41*, 2878-2890.

[15] R. E. Handschumacher, M. W. Harding, J. Rice, R. J. Drugge, D. W. Speicher, *Science* **1984**, *226*, 544-547.

[16] E. M. Driggers, S. P. Hale, J. Lee, N. K. Terrett, *Nat Rev Drug Discov* **2008**, *7*, 608-624.

[17] H. He, J. Guo, J. Xu, J. Wang, S. Liu, B. Xu, *Nano letters* **2021**, *21*, 4078-4085.

[18] N. Matsumori, N. Yamaji, S. Matsuoka, T. Oishi, M. Murata, *Journal of the American Chemical Society* **2002**, *124*, 4180-4181.

[19] a) A. G. Barrett, A. J. Hennessy, R. L. Vézouët, P. A. Procopiou, P. W. Seale, S. Stefaniak, R. J. Upton, A. J. White, D. J. Williams, *The Journal of organic chemistry* **2004**, *69*, 1028-1037; b) L. V. Bonaga, H.-C. Zhang, A. F. Moretto, H. Ye, D. A. Gauthier, J. Li, G. C. Leo, B. E. Maryanoff, *Journal of the American Chemical Society* **2005**, *127*, 3473-3485.

[20] a) D. Al Kelabi, A. Dey, L. O. Alimi, H. Piwoński, S. Habuchi, N. M. Khashab, *Chemical science* **2022**, *13*, 7341-7346; b) L. O. Alimi, F. Fang, B. Moosa, Y. Ding, N. M. Khashab, *Angewandte Chemie* **2022,** 134, 43, e202212596 ; c) Y. Ding, L. O. Alimi, B. Moosa, C. Maaliki, J. Jacquemin, F. Huang, N. M. Khashab, *Chemical science* **2021**, *12*, 5315-5318; d) T. Hasell, A. I. Cooper, *Nature Reviews Materials* **2016**, *1*, 16053; e) M. Mastalerz, *Acc Chem Res* **2018**, *51*, 2411-2422.

[21] a) T. Rezai, J. E. Bock, M. V. Zhou, C. Kalyanaraman, R. S. Lokey, M. P. Jacobson, *Journal of the American Chemical Society* **2006**, *128*, 14073-14080; b) T. Rezai, B. Yu, G. L. Millhauser, M. P. Jacobson, R. S. Lokey, *Journal of the American Chemical Society* **2006**, *128*, 2510-2511.

[22] M. Kaur, D. Choi, *Chemical Society reviews* **2015**, *44 1*, 58-77.

[23] S. E. Gibson, C. Lecci, *Angewandte Chemie International Edition* **2006**, *45*, 1364-1377.

[24] T. Zou, C.-N. Lok, Y. M. E. Fung, C.-M. Che, *Chemical Communications* **2013**, *49*, 5423-5425.

[25] P. G. Dougherty, A. Sahni, D. Pei, *Chemical Reviews* **2019**, *119*, 10241-10287.

[26] N. Chen, Y. He, M. Zang, Y. Zhang, H. Lu, Q. Zhao, S. Wang, Y. Gao, *Biomaterials* **2022**, *286*, 121567.

[27] C. Liu, T. Wan, H. Wang, S. Zhang, Y. Ping, Y. Cheng, *Science Advances* **2019**, *5*, eaaw8922.

[28] D. S. Bindels, L. Haarbosch, L. van Weeren, M. Postma, K. E. Wiese, M. Mastop, S. Aumonier, G. Gotthard, A. Royant, M. A. Hink, T. W. J. Gadella, *Nature Methods* **2017**, *14*, 53-56.

[29] S. Mahanta, S. Paul, A. Srivastava, A. Pastor, B. Kundu, T. K. Chaudhuri, *Colloids and Surfaces B: Biointerfaces* **2015**, *130*, 237-245.

[30] H. Nishimasu, L. Cong, Winston X. Yan, F. A. Ran, B. Zetsche, Y. Li, A. Kurabayashi, R. Ishitani, F. Zhang, O. Nureki, *Cell* **2015**, *162*, 1113-1126.

[31] L. Li, J. O. Fierer, T. A. Rapoport, M. Howarth, *Journal of Molecular Biology* **2014**, *426*, 309-317.

[32] E. Díaz-Galicia, R. Grünberg, S. T. Arold, *Biosensors* **2022**, *12*, 53.

[33] Y. Yan, H. Tao, S. Y. Huang, *Nucleic Acids Res* **2018**, *46*, W423-w431.

[34] C. Dominguez, R. Boelens, A. M. Bonvin, *J Am Chem Soc* **2003**, *125*, 1731-1737.

10.1002/anie.202403647

[35] a) B. Kulkarni, S. Qutub, N. M. Khashab, N. Hadjichristidis, *ACS Omega* **2023**, *8*, 22698-22707; b) V. K. Mutalik, J. C. Guimaraes, G. Cambray, C. Lam, M. J. Christoffersen, Q. A. Mai, A. B. Tran, M. Paull, J. D. Keasling, A. P. Arkin, D. Endy, *Nat Methods* **2013**, *10*, 354-360; c) S. C. Strutt, R. M. Torrez, E. Kaya, O. A. Negrete, J. A. Doudna, *Elife* **2018**, 5;7:e32724.

10.1002/anie.202403647

TOC

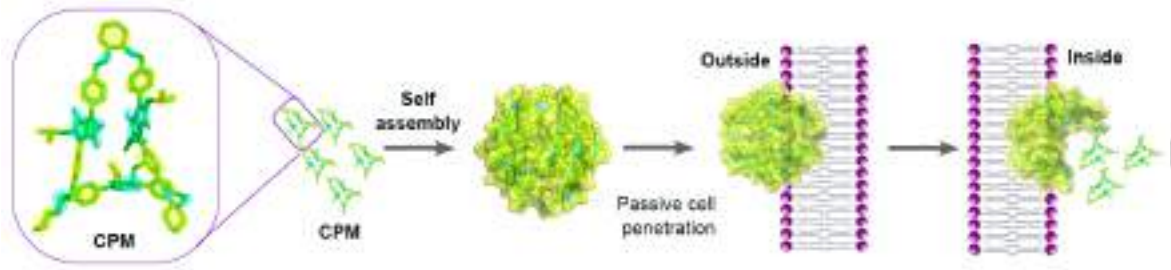

A cell penetrating macrocycle (CPM) with flexible amine linkages and amphiphilic nature assembles into a micellar-like structure that can passively permeate through the cell membrane. CPMs can efficiently transfer fully functioning proteins and genetic materials into the cytosol, independent of size, charge, or complexity.

Institute and/or researcher Twitter usernames: @KAUST_PSE

Twitter: Khashab Group-ShmsLab (@ShmsLab)